The color-adjustable phosphor $Sr_4La(PO_4)_3O:Ce^{3+},Tb^{3+},Mn^{2+}$ of WLEDs: luminescence and transfer of energy characteristics

Phuc Dang Huu[1], Phan Xuan Le[2]

[1]Faculty of Fundamental Science, Industrial University of Ho Chi Minh City, Ho Chi Minh City, Vietnam
[2]Faculty of Mechanical-Electrical and Computer Engineering, School of Engineering and Technology, Van Lang University, Ho Chi Minh City, Vietnam

ABSTRACT

A high heat solid-state technique was used to produce a set of phosphor $Sr_4La(PO_4)_3O:Ce^{3+},Tb^{3+},Mn^{2+}$ (Sr:Mn). In $Sr_4La(PO_4)_3O$, the luminescence characteristics, heat resistance, and energy conversion between Ce^{3+} and Tb^{3+} as well as Mn^{2+} were thoroughly researched. Introducing the activator Ce^{3+} particles can significantly increase the dim green-emitting from Tb^{3+} and the red-emitting from Mn via energy conversion. The color of the emissions might be changed by adjusting the Ce^{3+}/Tb^{3+} and Ce^{3+}/Mn^{2+} ion ratios. In the $Sr_4La(PO_4)_3O$: 0.12 Ce^{3+},0.3 Mnz^{2+} specimen, we achieved white-emitting illumination, yielding hue coefficients (0.3326, 0.3298), showing that the phosphor Sr:Mn could have promising implications for white light-emitting diodes (WLEDs).

Corresponding Author:

Phan Xuan Le
Faculty of Mechanical-Electrical and Computer Engineering, School of Engineering and Technology
Van Lang University
Ho Chi Minh City, Vietnam
Email: le.px@vlu.edu.vn

1. INTRODUCTION

White light-emitting diode (WLED) devices would be commonly employed and have sparked a lot of commercial interest as solid-state illumination because of their extended duration, energy efficiency, compact size, and environmental friendliness [1], [2]. Pairing a blue-light indium gallium nitride (InGaN) chip with a $Y_3Al_5O_{12}:Ce^{3+}$ (YAG:Ce) phosphor that emits yellow light is now the most common approach to produce white-emitting light [3]. As the red-light proportion is not sufficient, this type of white output has an insignificant color-rendering index (CRI) of roughly between 70 and 80 as well as a great correlated hue temperature (CCT) of roughly 7500 K [4], [5]. Many scientists have claimed that the phosphors emitting red lighting could be triggered by phosphors emitting blue lighting in the past years. $Na_5Ln(MoO_4)_4:Eu^{3+}$ (Ln=La, Gd, Y) [6], $CaS:Eu^{2+}$ [7], $CaAlSiN_3:Eu^{2+}$ [8], and $K_2SiF_6:Mn^{4+}$ [9], [10] are examples of these kind of phosphors. The phosphorus transformed WLEDs could have poor CCT and excellent CRI using these phosphors. However, weak blue emission efficacies resulting from severe re-absorption between the phosphors emitting green and red light, as well as costly production, are two major issues. As a result, several researchers have concentrated on producing quality, long-lasting, single-stage white emitting phosphors comprising red, green, and blue (RGB) elements using the energy transference (ET) process across sensitizes to activators [11]-[13].

Co-doping Ce^{3+}, Tb^{3+} or Mn^{2+} particles in single-stage phosphors is typical for achieving white light emission using ET in many WLED types of phosphors. Ce^{3+} contains a $4f^15d^0$ ground state and a $4f^05d^1$

excited state, indicating typical 5d-4f electronic conversions. Since the Ce^{3+} power levels dispersion is under the dramatic impact imposed by the host lattice, emission from the 5d-4f conversion can occur over a wide wavelength band. The particles Tb^{3+} and Mn^{2+} have been employed accordingly as green and red emission elements in the past. Yet, owing to the banned 4f-4f transfer of Tb^{3+} and $^4T_1$-$^6A_1$ shift of Mn^{2+}, the excited bands of Tb^{3+} and Mn^{2+} particles across ultraviolet (UV) to the visible area are relatively faint [14], [15]. To increase the absorption of Tb^{3+} and Mn^{2+} in the UV area, a common way is to add an effective sensitizer, such as Ce^{3+}, and transmit the highly absorbed excited power from Ce^{3+}'s 5d level to Tb^{3+}'s $^5D_{3,4}$ level or Mn^{2+}'s fourth-generation (4G) level [16], [17]. This method is suitable for making emission-tunable single-stage phosphors, which have benefits such as decreased production expenses, excellent color consistency, and great luminescence efficacy [18], [19]. Apatites have proven to be excellent major ingredients when producing phosphors up to this point as they possess considerable mechanical and chemical durability. $Sr_4La(PO_4)_3O$ (SLPO) is an apatite complex having two cation locations: a nine-fold coordinating 4f location having C_3 point symmetry along with a seven-fold coordinating six h location with C_s point symmetry [20]. The SLPO: Eu^{3+}/Tb^{3+}/Ce^{3+} phosphors were investigated in an earlier piece of research [21]. Tb^{3+} and Mn^{2+} were incorporated to SLPO:Ce^{3+} in this study. ET could generate a Tb^{3+} green emission peak of 539 nm and a Mn^{2+} red emission maximum of roughly 605 nm. Between Ce^{3+} and Tb^{3+} as well as Mn^{2+}, their photoluminescence and ET characteristics were extensively investigated. Tunable emitting colors between blue to green and mild white have been achieved by altering the dopant concentration of Tb^{3+} or Mn^{2+}, implying a prospective use in UV-pumped WLEDs.

2. COMPUTATIONAL SIMULATION

2.1. Creating SrMn phosphor with green illumination

Traditional extreme temperatures solid-state processes were used to make $Sr_4La_{1-x-y}(PO_4)_3O$:xCe^{3+},yTb^{3+} and $Sr_{4-z}La_{1-x}(PO_4)_3O$:$xCe^{3+}$,$zMn^{2+}$ phosphors with various compositions. $SrCO_3$, $(NH_4)_2HPO_4$, and $MnCO_3$ (99.99%) with La_2O_3, Tb_4O_7, and CeO_2 (99.99%) were among the beginning materials. As a flux, 2 wt% Li_2CO_3 (99%) was added. An agate mortar was used to combine and grind the stoichiometric initiating reagents completely. The combination was pre-heated for 3 hours in air at 600 °C, re-pulverized, and calcined within a decreasing environment (N_2:H_2=95:5) for 5 hours at 1200 °C. An AL X'TRA powder X-ray diffractometer (XRD) with Cu Kα radiation (λ=1.5406 Å) running under 40 kilovolts as well as 35 milliamperes was used to measure phase purity. Disperse reflection spectrum (DRS) between 200 and 700 nm were acquired via an UV/visible spectrophotometer with $BaSO_4$ as a guide. We employed a field emission detecting electronmicroscope for the task of identifying the forms of the as-prepared specimens field emission scanning electron microscope, field emission gun (FESEM, FEI, Quanta FEG). On an FS5 fluorescent spectrometer possessing a xenon light operating at 150 watts as illumination, the photoluminescence stimulation (PLE) and photoluminescence (PL) spectrum were obtained. The specimens were placed above a system that could be fired from 25 to 200 °C with a 1 °C stage, and the thermally activated measurement was conducted by the FS5 spectrometer mechanism. Using an integrated sphere in the FS5 spectrometer, the specimens' photoluminescence external quantum outputs were determined. An fluorescence spectrometer (FLS) 920 was used to measure the fluorescence lifespan [22].

2.2. Transferring energy and luminous characteristics in SrMn

The absorption spectra of SLPO were derived from the reflecting spectra utilizing the Kubelka-Munk (K-M) function to calculate the SLPO combination optic bandgap value analytically [23].

$$F(R) = \frac{(1-R)^2}{2R} = K/S \qquad (1)$$

The reflections, absorbance, and scattering coefficients are R, K, and S, correspondingly. The Tauc relation connects the bandgap E_g and linearly absorbing factors of a substance:

$$\alpha hV \propto \left(hV - E_g\right)^{n/2} \qquad (2)$$

in which n=1, 2, 3, 4, and 6 correspond to direct permitted transition processes, non-metal substances, direct prohibited transition processes, indirect permitted transition processes, and indirect prohibited transition processes [24]. As the substance distributes in a fully diffused pattern, the absorbing factor K is 2α. Because the diffusing parameter S is fixed in relation to wavelength, we can utilize (1) and (2) to get (3)

$$[F(R)hV]^2 \propto \left(hV - E_g\right)^n \qquad (3)$$

The optimum straight matching around the absorbing edge may be attained by $n=2$ throughout the plots of $[F(R)hv]^2$, $[F(R)hv]$, $[F(R)hv]^{2/3}$, $[F(R)hv]^{1/2}$, and $[F(R)hv]^{1/3}$ through the power of photon hv. The plot of $[F(R)hv]$ versus hv is illustrated via Figure 1. The SLPO optic bandgap (3.85eV) can be calculated by extending the straight match to $[F(R)hv]=0$.

The phosphorous film in genuine multi-chip white LEDs (MCW-LEDs) is reproduced using flattened silicon films by the LightTools 9.0 application with the Monte Carlo approach. This modeling occurs across two distinct durations: 1) it is essential to determine and create MCW-LED light configuration prototypes and 2) optical properties. The optical impacts of the phosphorous compound are therefore properly regulated by the SrMn concentration variation. We must develop some comparisons to examine the effect of YAG:Ce^{3+} and SrMn phosphorous compounds on the performance of MCW-LED lights. Double-layer distant phosphorus, described as two types of compounds with median central conduction times (CCTs) at 3000 K, 4000 K, and 5000 K, is explained. Figure 1 depicts MCW-LED lights featuring conformal phosphorous compound and an 8500-K median CCT in detail. The MCW-LEDs modeling without SrMn is also recommended. The reflector's floor length, height, and surface area length are 8, 2.07, and 9.85 in millimeters, respectively. The conformal phosphorous compound is applied to nine 0.08 mm thick chips. Every LED chip is linked to the reflector cavity, which is 0.15 mm high, by a 1.14 mm^2 square base region. Each blue-color chip yields an illuminating output measured at 1.16 W as well as a maximum wavelength measured at 453 nm.

Figure 1. Picture depicting a WLED device

3. RESULTS AND DISCUSSION

Figure 2 presents the reversal change in the concentrations of green-emitting SrMn and yellow-emitting YAG:Ce^{3+} phosphors, under CCTs of 5000 K and 6500 K in Figure 2(a) and (b), respectively. The change has two functions: retaining median CCTs and impacting WLEDs emission and absorption with dual phosphorus layers. This, in turn, can affect WLEDs' color quality and luminous flux efficacy. WLEDs' color quality is therefore determined by the SrMn concentration specified. As the SrMn ratio increases 2%-20% Wt., the content of YAG:Ce^{3+} reduces to keep the median CCTs. This is also true for WLEDs with hue heats ranging between 5600 K and 8500 K.

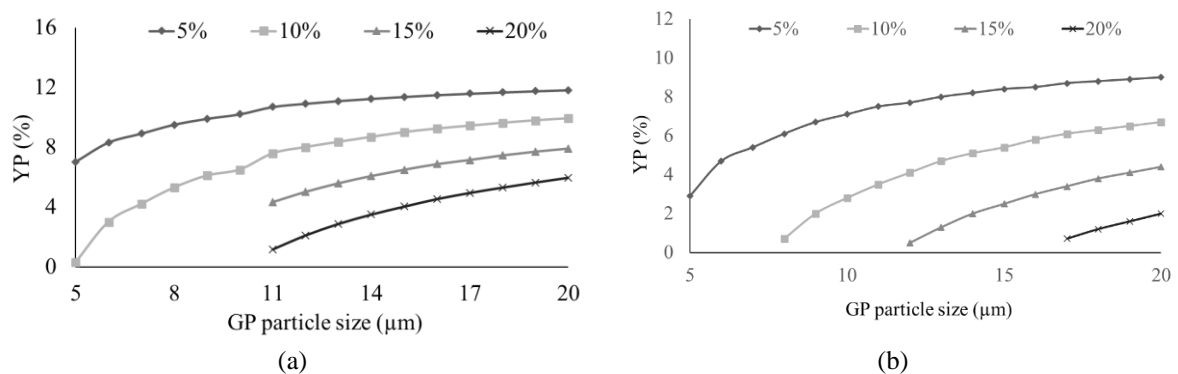(a)   (b)

Figure 2. The preservation of the median CCT by modifying the phosphorus concentration: (a) 5000 K and (b) 6500 K

The influence imposed by the SrMn concentration on the WLEDs transmission bands of colors is demonstrated by Figure 3, under CCTs of 5000 K and 6500 K in Figures 3(a) and (b), respectively. The choices made will depend on the industry standards. WLED devices which offers decent hue fidelity will yield a slight lumen penalty. White-emitting illumination results from the spectrum zone's composition, as demonstrated by Figure 3. The 5000 K spectrum is shown in this diagram. The brilliance trend increases as SrMn concentration in two light spectrums: 420 nm-480 nm along with 500 nm-640 nm. The luminous flux enhancement may be seen in the two-band emitting spectra. Furthermore, blue-light dispersion in WLEDs is enhanced, indicating that diffusing in the phosphorus film and WLEDs is augmented as well, supporting color homogeneity. As SrMn takes part in the process, the said result can be noteworthy. The hue consistency from the great heat distant phosphorus configuration, particularly, is challenging to manage. This analysis revealed that SrMn, under maximum (8500 K) as well as minimum (8500 K) hue temperatures, will boost WLEDs' hue standard.
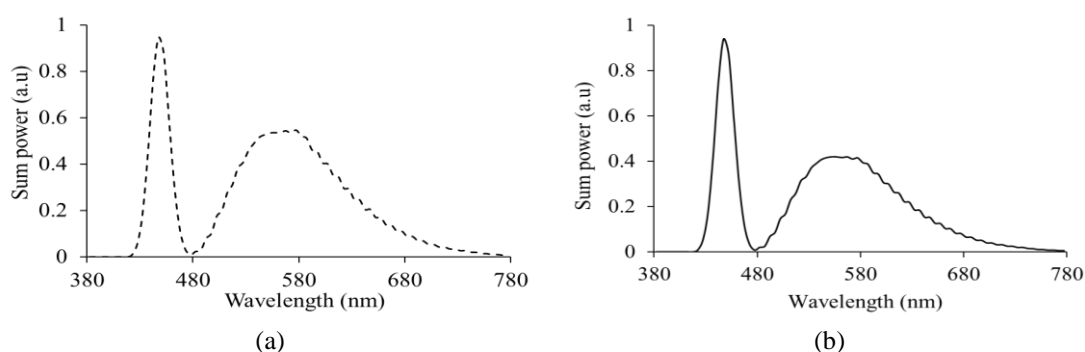

Figure 3. The correlation between SrMn content and WLEDs discharge spectrum: (a) 5000 K and (b) 6500 K

The lumen efficacy of the dual-sheet remote phosphorus layout was thereby demonstrated in the study. The findings in Figure 4 indicate that as the SrMn concentration grew 2% wt-20% wt, the illumination radiated rose dramatically, under CCTs of 5000 K and 6500 K in Figures 4(a) and (b), respectively. The color variation was massively diminished with SrMn concentration in the three median CCTs, per Figure 5 with Figures 5(a) and (b) depicting the results under 5000 K and 6500 K, respectively. This is indicated by the absorbing nature in the red-color phosphorous film. The blue illumination from the LED chip is converted to green as it is absorbed by the SrMn. The SrMn ions absorb the yellow as well as the blue light component from the chip. The blue lighting absorptivity from the LED chip displays more potency, surpassing the aforementioned absorptions, a result of the absorbing capabilities in the substance. SrMn boosts the green light component in WLEDs, which improves the color homogeneity index. Color uniformity is among the essential facets of current WLED light criteria. The higher the color uniformity value, the higher the cost of WLED white light. Yet, the insignificant price of SrMn is a plus. SrMn could indeed have a variety of applications.
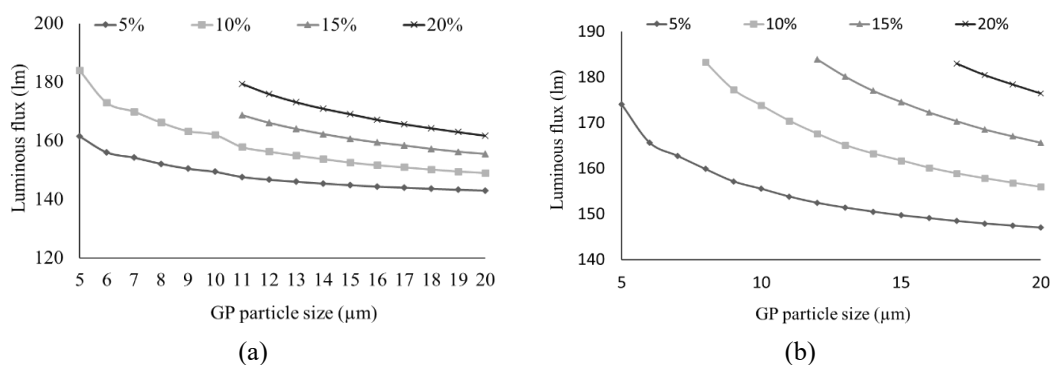

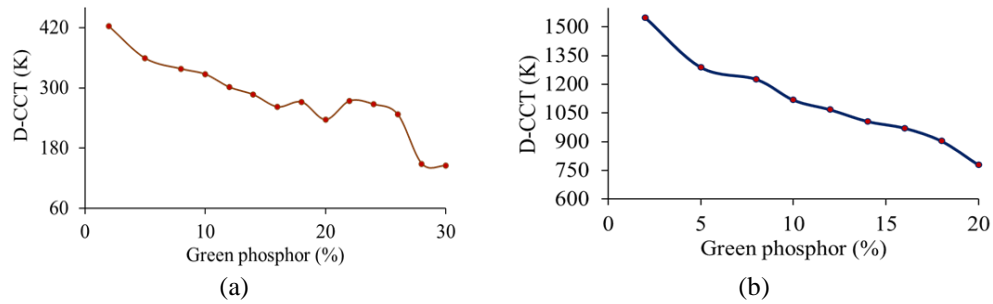Figure 4. SrMn concentration functions as WLEDs luminous flux: (a) 5000 K and (b) 6500 K

Figure 5. SrMn concentration functions as WLEDs color deviation (a) 5000 K and (b) 6500 K

Hue consistency would be the sole factor for evaluating hue fidelity in WLED devices. Color output cannot be claimed to be acceptable with such a high color uniformity value. As a result, current research works have proposed a CRI and a color quality scale (CQS). When illuminated, the hue rendering factor determines the actual hue of an item [25]. The abnormal green illumination volume related to the principal hues: blue, yellow, and green, causes color imbalance. This causes inferior hue consistency for WLEDs. The results in Figure 6 show a slight decline in CRI in the remote phosphor SrMn layer addition, under CCTs of 5000 K and 6500 K in Figures 6(a) and (b), respectively. Nonetheless, the flaws should be tolerable. In comparison to CRI, CQS should be favored. On the other hand, it can be challenging when it comes to attaining this parameter. CQS comprises certain factors: CRI, user's preference, and hue coordinates. With these essential factors, CQS is becoming a genuine overall hue standard assessment. Figure 7 shows the CQS increase when the remote phosphor SrMn layer is present, under CCTs of 5000 K and 6500 K in Figures 7(a) and (b), respectively. Furthermore, CQS does not differ accordingly as the SrMn concentration is under 10% wt. CRI and CQS would considerably decline as SrMn content raises above 10% wt. because of strong discoloration when the color of green is dominating. Because of this, if green phosphor SrMn is used, proper concentration selection would be critical.
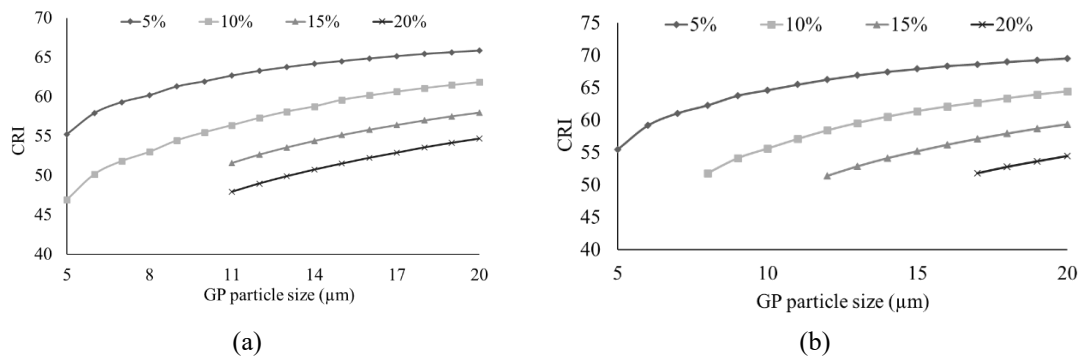

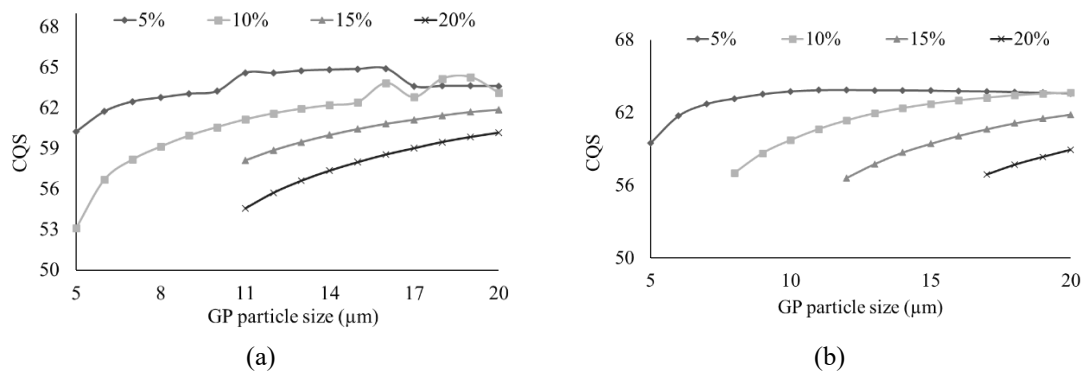Figure 6. SrMn concentration functions as WLEDs color rendering index (a) 5000 K and (b) 6500 K

Figure 7. SrMn concentration functions as WLEDs color quality scale (a) 5000 K and (b) 6500 K

4. CONCLUSION

The effect of green SrMn phosphorus on the double-layer phosphor arrangement's optical properties is discussed in this work. The analysis revealed that SrMn is a great option for enhancing hue homogeneity utilizing Monte Carlo mathematical models. This is true for WLEDs, which have a poor 5000 K color temperature as well as a color heat exceeding 8500 K. The outcomes of this article have achieved the objective of improving the hue standard and illuminating beams, which is a challenging process due to the remote phosphor structure. But both CRI and CQS have a tiny drawback. The CRI and CQS fall dramatically as the SrMn concentration is enhanced substantially. Hence, the right concentration must be determined depending on the manufacturer's goals. The research has provided a wealth of helpful data for generating higher WLEDs color uniformity and luminous flux. The typical solid-state procedure was used to make a set of SLPO: $0.12Ce^{3+}$, yTb^{3+} and SLPO: $0.12Ce^{3+}$, zMn^{2+} phosphors. The ETs between Ce^{3+} and Tb^{3+} as well as Ce^{3+} to Mn^{2+} were thoroughly investigated. Dipole-dipole interactions governed the processes of the two ETs. The concentration of Tb^{3+} or Mn^{2+} particles can be adjusted to produce a variety of emission colors ranging between greenish-blue and green or mild white. Under the 310 nm excitation of UV-light, white lighting radiation featuring a CIE result shown as (0.3326, 0.3298) may be generated by the SLPO: $0.12Ce^{3+}$, $0.3Mn^{2+}$ phosphor. Because of advancements in technics using semiconductivity, the chips for synthesizing phosphors within LEDs may now be made using a variety of emitted wavelengths, indicating that the SLPO: $Ce^{3+}/Tb^{3+}/Mn^{2+}$ is a promising single-composition phosphor of white LED apparatuses.

REFERENCES

[1] H. Yuce, T. Guner, S. Balci, and M. M. Demir, "Phosphor-based white LED by various glassy particles: Control over luminous efficiency," *Opt. Lett*, vol. 44, no. 3, pp. 479-482, 2019, doi: 10.1364/OL.44.000479.

[2] J. Chen, B. Fritz, G. Liang, X. Ding, U. Lemmer, and G. Gomard, "Microlens arrays with adjustable aspect ratio fabricated by electrowetting and their application to correlated color temperature tunable light-emitting diodes," *Opt. Express*, vol. 27, no. 4, pp. A25-A38, 2019, doi: 10.1364/OE.27.000A25.

[3] H. Jia *et al.*, "High-transmission polarization-dependent active plasmonic color filters," *Appl. Opt.*, vol. 58, no. 3, pp. 704-711, 2019, doi: 10.1364/AO.58.000704.

[4] B. K. Tsai, C. C. Cooksey, D. W. Allen, C. C. White, E. Byrd, and D. Jacobs, "Exposure study on UV-induced degradation of PTFE and ceramic optical diffusers," *Appl. Opt.*, vol. 58, no. 5, pp. 1215-1222, 2019, doi: 10.1364/AO.58.001215.

[5] A. Ahmad, A. Kumar, V. Dubey, A. Butola, B. S. Ahluwalia, and D. S. Mehta, "Characterization of color cross-talk of CCD detectors and its influence in multispectral quantitative phase imaging," *Opt. Express*, vol. 27, no. 4, pp. 4572-4589, 2019, doi: 10.1364/OE.27.004572.

[6] M. Talone and G. Zibordi, "Spatial uniformity of the spectral radiance by white LED-based flat-fields," *OSA Continuum*, vol. 3, no. 9, pp. 2501-2511, 2020, doi: 10.1364/OSAC.394805.

[7] W. Zhong, J. Liu, D. Hua, S. Guo, K. Yan, and C. Zhang, "White LED light source radar system for multi-wavelength remote sensing measurement of atmospheric aerosols," *Appl. Opt.*, vol. 58, no. 31, pp. 8542-8548, 2019, doi: 10.1364/AO.58.008542.

[8] J. Kim, H. S. Jo, and U. C. Ryu, "Improving CRI and Scotopic-to-Photopic Ratio Simultaneously by Spectral Combinations of CCT-tunable LED Lighting Composed of Multi-chip LEDs," *Curr. Opt. Photon.*, vol. 4, no. 3, pp. 247-252, 2020, doi: 10.3807/COPP.2020.4.3.247.

[9] Y. Zhou *et al.*, "Comparison of nonlinear equalizers for high-speed visible light communication utilizing silicon substrate phosphorescent white LED," *Opt. Express*, vol. 28, no. 2, pp. 2302-2316, 2020, doi: 10.1364/OE.383775.

[10] Q. Xu, L. Meng, and X. Wang, "Nanocrystal-filled polymer for improving angular color uniformity of phosphor-converted white LEDs," *Appl. Opt.*, vol. 58, no. 27, pp. 7649-7654, 2019, doi: 10.1364/AO.58.007649.

[11] G. Zhang, K. Ding, G. He, and P. Zhong, "Spectral optimization of color temperature tunable white LEDs with red LEDs instead of phosphor for an excellent IES color fidelity index," *OSA Continuum*, vol. 2, no. 4, pp. 1056-1064, 2019, doi: 10.1364/OSAC.2.001056.

[12] B. Zhao, Q. Xu, and M. R. Luo, "Color difference evaluation for wide-color-gamut displays," *J. Opt. Soc. Am.*, vol. 37, no. 8, pp. 1257-1265, 2020, doi: 10.1364/JOSAA.394132.

[13] A. Udupa, X. Yu, L. Edwards, and L. L. Goddard, "Selective area formation of arsenic oxide-rich octahedral microcrystals during photochemical etching of n-type GaAs," *Opt. Mater. Express*, vol. 8, no. 8, pp. 289-294, 2018, doi: 10.1364/OME.8.000289.

[14] X. Li *et al.*, "Highly stable and tunable white luminescence from Ag-Eu³⁺ co-doped fluoroborate glass phosphors combined with violet LED," *Opt. Express*, vol. 26, no. 2, pp. 1870-1881, 2018, doi: 10.1364/OE.26.001870.

[15] S. Sadeghi, B. G. Kumar, R. Melikov, M. M. Aria, H. B. Jalali, and S. Nizamoglu, "Quantum dot white LEDs with high luminous efficiency," *Optica*, vol. 5, no. 7, pp. 793-802, 2018, doi: 10.1364/OPTICA.5.000793.

[16] T. Wang, "Electrically Injected Hybrid III-Nitride/Organic White LEDs with Nonradiative Energy," *OSA Technical Digest*, pp. W2J, 2018, doi: 10.1364/CLEOPR.2018.W2J.1.

[17] C. Zhang, L. Xiao, P. Zhong, and G. He, "Photometric optimization and comparison of hybrid white LEDs for mesopic road lighting," *Applied Optics*, vol. 57, no. 16, pp. 4665-4671, 2018, doi: 10.1364/AO.57.004665.

[18] A. Vaskuri *et al.*, "Relationships between junction temperature, electroluminescence spectrum and ageing of light-emitting diodes," *Metrologia*, vol. 55, no. 2, 2018, doi: 10.1088/1681-7575/aaaed2.

[19] W. Shiyu, S. Yan, and Z. Yi, "Color Temperature adjustable LED based on Structured fluorescent film," *OSA Technical Digest*, pp. Su2A.272, 2018, doi: 10.1109/ACP.2018.8595763.

[20] Y. Peng *et al.*, "Flexible fabrication of a patterned red phosphor layer on a YAG:Ce^{3+} phosphor-in-glass for high-power WLEDs," *Opt. Mater. Express*, vol 8, no. 3, pp. 605-614, 2018, doi: 10.1364/OME.8.000605.
[21] L. Duan and Z. Lei, "Wide color gamut display with white and emerald backlighting," *Appl. Opt.*, vol. 57, no. 6, pp. 1338-1344, 2018, doi: 10.1364/AO.57.001338.
[22] H. P. Huang, M. Wei, and L. C. Ou, "White appearance of a tablet display under different ambient lighting conditions," *Opt. Express*, vol. 26, no. 4, pp. 5018-5030, 2018, doi: 10.1364/OE.26.005018.
[23] Z. Li, Y. Tang, J. Li, X. Ding, C. Yan, and B. Yu, "Effect of flip-chip height on the optical performance of conformal white-light-emitting diodes," *Opt. Lett.*, vol. 43, no. 5, pp. 1015-1018, 2018, doi: 10.1364/OL.43.001015.
[24] L. Xiao, C. Zhang, P. Zhong, and G. He, "Spectral optimization of phosphor-coated white LED for road lighting based on the mesopic limited luminous efficacy and IES color fidelity index," *Applied Optics*, vol. 57, no. 4, pp. 931-936, 2018, doi: 10.1364/AO.57.000931.
[25] W. L. Chiong, A. F. Omar, M. Z. M. Jafri, and C. H. Tan, "Spectroscopic Col our Evaluation under Different White Light Emitting Diode Illumination Angle," *Journal of Physics: Conference Series*, vol. 1083, no 1, 2018, doi: 10.1088/1742-6596/1083/1/012023.

BIOGRAPHIES OF AUTHORS

Phuc Dang Huu received a Physics Ph.D degree from the University of Science, Ho Chi Minh City, in 2018. Currently, he is a lecturer at the Faculty of Fundamental Science, Industrial University of Ho Chi Minh City, Ho Chi Minh City, Vietnam. His research interests include simulation LEDs material and renewable energy. He can be contacted at email: danghuuphuc@iuh.edu.vn.

Phan Xuan Le received a Ph.D. in Mechanical and Electrical Engineering from Kunming University of Science and Technology, Kunming city, Yunnan province, China. Currently, He is a lecturer at the Faculty of Engineering, Van Lang University, Ho Chi Minh City, Viet Nam. His research interests are optoelectronics (LED), power transmission and automation equipment. He can be contacted at email: le.px@vlu.edu.vn.